

Anomalous diffusion and effective shear modulus in a semi-solid membrane

Vikash Pandey¹ and Dhrubaditya Mitra¹

¹*NORDITA, KTH Royal Institute of Technology and Stockholm University,
Hannes Alfvéns väg 12, 10691 Stockholm, Sweden*

From the perspective of physical properties, the cell membrane is an exotic two-dimensional material that has a dual nature: it exhibits characteristics of fluids, i.e., lipid molecules show lateral diffusion, while also demonstrating properties of solids, evidenced by a non-zero shear modulus. We construct a model for such a *semi-solid membrane*. Our model is a fluctuating randomly triangulated mesh with two different kinds of nodes. The solid nodes never change their neighbors, while the fluid nodes do. As the area fraction occupied by the solid nodes (Φ) is increased the motion of fluid nodes transition from diffusion to localization via subdiffusion. Next, the solid nodes are pinned to mimic the pinning of the plasma membrane to the cytoskeleton. For the pinned membrane, there exists a range of Φ over which the model has both a non-zero shear modulus and a non-zero lateral diffusivity. The bending modulus, measured through the spectrum of height fluctuations remains unchanged.

The building block of all organisms is the cell. The cell membrane forms a barrier that separates the cytoplasm from the external environment. Composition wise, a typical cell membrane is approximately 73% lipid molecules and about 23% proteins [1]. The canonical model of cell membrane is the fluid mosaic model, proposed by Singer and Nicolson [2], who conceptualized it as a fluid membrane with two leafs made of lipids with diverse inclusions of proteins, carbohydrates, and cholesterol. The fluid membrane is modeled by the Helfrich energy functional [3–5] which has energy cost to bending and change in area but has zero shear elastic modulus. Minimizing this Hamiltonian with the constraint of fixed volume correctly captures the common biconcave shape of red blood cells (RBCs) [6–8]. Such a model can also be used to correctly interpret micro-pipette aspiration experiments [5]. However, to capture all the different shapes a RBC can have (e.g., discocyte, stomatocyte, and echinocyte) from a single model it is necessary to consider a composite model, as noted in Ref. [9],

“where the plasma membrane contributes bending rigidity and the protein-based membrane skeleton contributes stretch and shear elasticity.”

Furthermore, it is necessary to include shear elasticity in models of RBC’s to capture their shapes in microfluidic flows [10] and to interpret the results of mechanical deformation of RBCs in certain optical tweezer experiments [11–14]. Hence the consensus is that cell membrane of RBCs, and by extension all cells, have a shear modulus and this emerges due to coupling with the cytoskeleton. In contrast, a large body of experiments [15–22] show that the lateral motion of tagged lipid molecules in the cell membrane is diffusive, although the diffusion may be anomalous. This is typical feature of a (two-dimensional) fluid. Furthermore, the fact that the cell membrane forms tethers provides additional evidence in support of its fluid nature. Along similar lines, Shi *et al.* [23] have interpreted the mutual interaction of two tethers in a cell using a model where the cell membrane is

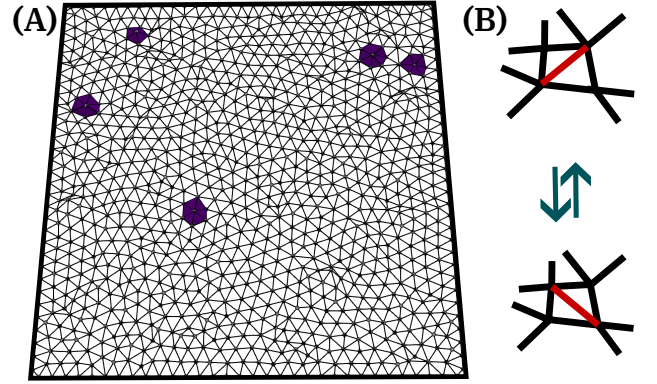


FIG. 1. (A) A representative picture of our model: it is a fluctuating, randomly triangulated surface where the solid regions are colored in purple. It is connected to a frame. (B) An example of bond flips that fluidize our membrane.

modeled as a porous media [24]. Thus, the cell membrane is an exotic two-dimensional material with physical properties akin to both solids and fluids. Here we present, for the first time, a minimal model that captures this dual nature.

We start with a model for isotropic and homogeneous two-dimensional elastic material. In the Monge gauge the deformation can be described by an in-plane vector $\mathbf{u}(x_1, x_2)$ and an out-of-plane displacement $f(x_1, x_2)$. The Hamiltonian is given by,

$$\mathcal{H} = \int d\mathbf{x} \left[\frac{\kappa}{2} (\nabla^2 f)^2 + \mu s_{\alpha\beta}^2 + \frac{\lambda}{2} s_{\alpha\alpha}^2 \right], \quad (1a)$$

$$\text{where } s_{\alpha\beta} \equiv \frac{1}{2} (\partial_\alpha u_\beta + \partial_\beta u_\alpha + \partial_\alpha f \partial_\beta f), \quad (1b)$$

is the strain tensor and μ and λ are the two Lamé coefficients [25, 26]. A possible Monte Carlo modeling of such a membrane [27–31] goes as follows. First, generate a random triangulated grid on a flat surface with N nodes, see Fig. (1A). Second, update the positions of the points (\mathbf{X}_i at node i) by discretizing the Hamiltonian in Eq. (1)

over this grid. The energy has two contribution,

$$E = E_S + E_B, \quad (2)$$

where the stretching and the bending contributions respectively are,

$$E_S = \frac{H}{2} \sum_{i,j} (\mathbf{X}_{ij} - \ell_{ij}^0)^2, \quad (3a)$$

$$\text{where } X_{ij} \equiv |\mathbf{X}_i - \mathbf{X}_j|, \quad (3b)$$

$$\text{and } E_B = \frac{\kappa}{2} \sum_i \mathcal{A}_i \mathbf{L}_i^2. \quad (3c)$$

The spring constant H sets the two Lamé coefficients [28, 32], \mathcal{A}_i is the area of the dual Voronoi cell at the node i and \mathbf{L}_i is the discretized Laplacian [27, 28, 30–33]. For the rest of this paper we shall call such a membrane *solid membrane* as it has a finite in-plane shear modulus. We use the Metropolis algorithm: we accept a move if it results in lowering the energy of the membrane; a move that increases the energy of the membrane by ΔE is accepted with the probability $\exp[-\Delta E/k_B T]$ where k_B is the Boltzmann constant and T is the temperature. We define a single Monte Carlo step as an attempt to move each of the N nodes at least once on average. Typically, our production runs use 10^6 Monte Carlo steps.

It is possible to *fluidize* this membrane in the following manner [see, e.g., 29, section 6.2.4]. After every M Monte Carlo steps we flip bonds between neighbors – bond between any two adjacent nodes is broken and a new bond between other points is formed as shown in Fig. (2B). This operation, is always allowed as long as the minimum number of neighbors of a node is greater than four and the length of new bond is less than a given maximum allowed bond length.

All the parameters used in this study, e.g., the number of nodes, the total number of Monte Carlo steps, etc, are given in (see Appendix A). To estimate the error we use BAGGING (Bootstrap AGGregation) [34] – the data (Γ) are divided into $n = 40$ subsets $\{\Gamma_1, \dots, \Gamma_n\}$. For any quantity, e.g., the total energy E , we calculate n mean values, where the k -th value is calculated by averaging over the data in Γ_k . The standard deviation calculated over all the sets is our error estimate.

The first novelty of our model is to randomly assign a fraction of total nodes to be *solid* and the rest of them to be fluid. By this we mean that the bonds of the solid nodes with their neighbors is never changed while the bonds between two fluid nodes can be exchanged. Changing the fraction Φ from 0 to 1 we go from a fluid membrane, to fluid membranes with solid inclusions and finally solid membrane. In Fig. (1A) the triangles formed by the solid points with their neighbors are colored. The fractions of area of the membrane that can be considered solid can be defined as $\Phi \equiv N_s^T/N^T$, where N_s^T is the number of triangles associated with the solid points and N^T is the total number of triangles. We study the physical properties of membrane as the Φ is changed.

We attach the nodes lying on the boundary of the membrane to a frame. The particles on the frame do not undergo any Monte Carlo move. By straining the frame we can impose an external strain on the membrane and calculate its response. Note that we do not include the triangles formed with the points on the frame in N^T .

In Fig. (2A) to (C) we show typical snapshots of strained membrane from our simulations. The panel (A) is for the fluid membrane ($\Phi = 0$) and the panel (C) is for the solid membrane ($\Phi = 1$). The panel (B) is for an intermediate value, $\Phi = 0.2$. The solid membrane shows a typical ridges that appear in sheared solid membranes, e.g., fabrics. In Fig. (2A) and (B) we allow bond exchange – for all nodes in (A) but for 80% nodes in (B). In Fig. (2D) to E we plot the trajectories of a (fraction of) nodes. In Fig. (2D) all the nodes are fluid. The nodes move by a large amount. From (D) to (E) the nodes get more and more localized. In (E), where no bond exchange is allowed, the nodes are completely localized.

In Fig. (3A) we plot the mean square displacement as a function of time (t),

$$\langle R^2(t) \rangle \equiv \langle [\mathbf{X}(t) - \mathbf{X}(0)]^2 \rangle, \quad (4)$$

where the symbol $\langle \cdot \rangle$ shows average over all the nodes. The fluid membrane, which corresponds to the top line, shows $\langle R^2 \rangle \sim t$, i.e., the nodes show diffusion. As the area fraction Φ increases we move from diffusion to subdiffusion ($\langle R^2 \rangle \sim t^\beta$ with $\beta < 1$) to the case of solid membrane where $\langle R^2 \rangle$ is constant at late times – a typical signature of localization. We estimate a Φ dependent diffusion constant by calculating

$$D(\Phi) \equiv \lim_{t \rightarrow \infty} \frac{\langle R^2 \rangle}{t} \quad (5)$$

Clearly there exists a critical value of Φ , Φ_c such that for $\Phi > \Phi_c$ the diffusion coefficient $D(\Phi) \approx 0$.

Henceforth, we will use the mean bond length for the initial grid, $b \equiv \langle \ell_{ij}^0 \rangle$ as our unit of length. We use the number of Monte Carlo steps as time and use $\tau \equiv b^2/D(\Phi = 0)$ as the unit of time. Energy is measured in the unit of $k_B T$. In these units the diffusion constant for the fluid membrane $D(\Phi = 0) = 1$.

Measurement of lateral diffusion constant of lipids on giant unilamellar vesicles (GUVs) which are reinforced with a network of polymeric filaments (e.g., actin filaments) shows [35–37] that the diffusion constant decreases as the coupling with the polymer network increases. Our model reproduces this result qualitatively. Heinemann *et al.* [36] models this phenomena with random walkers confined within cages created by random network in two dimensions. The walkers are allowed to jump across cage barriers with a certain probability. In contrast, in our model, it is the fluid nodes of the network that does the random walk while the solid patches acts as impenetrable barriers.

We also calculate the cumulative probability distribution function (CDF) of first-passage time for the

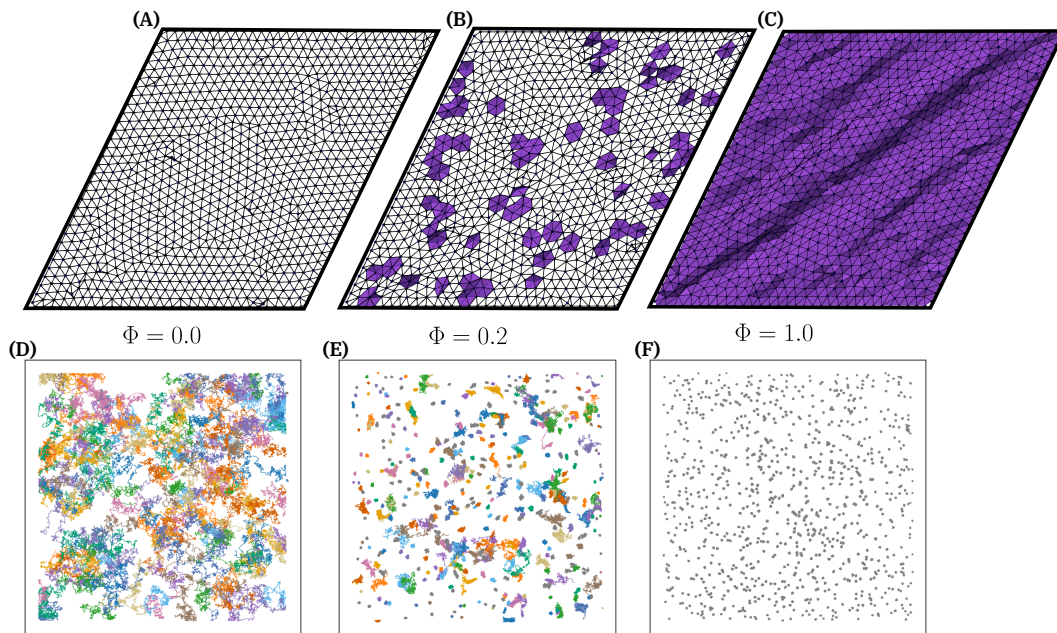


FIG. 2. (Top panel) Typical snapshots of sheared membranes from our simulations. The area fraction occupied by solid inclusion is Φ . From left to right: (A) $\Phi = 0$ (fluid membrane), (B) $\Phi = 0.2$ (fluid with solid inclusions), and (C) $\Phi = 1$ (solid membrane) which shows ridges typical of sheared fabric. The purple patches in the middle figure represent the solid regions. (Bottom panel) Representative trajectories of the nodes for the same three values of Φ .

fluid nodes. The CDF has exponential tails ((see Appendix B 1)) which implies that the probability distribution functions (PDF) of first-passage times also have exponential tails. This suggests that the anomalous diffusion we observe is not a continuous time random walk (CTRW) in which case the PDF of first-passage times show power-law tails [38, 39].

The anomalous diffusion we observe is akin to diffusion in crowded environment in two dimensions [22, 40], where depending on the fraction of area covered by the obstacles, the motion of Brownian particles go from diffusion to subdiffusion for intermediate times [40, 41]. At very late times the subdiffusive trajectories either becomes diffusive or gets localized ($D \rightarrow 0$) [41, 42]. As our membrane is bounded by a frame we cannot investigate whether the subdiffusion that we observe goes over to diffusion at late times or not. Saxton [42] and Sung and Yethiraj [43] have previously modeled the anomalous diffusion of tagged molecules in membranes in lattice and continuum models respectively. These models have certain qualitative similarities to our model but there are crucial quantitative differences (see Appendix B).

In Fig. (3B) we plot the self-intermediate scattering function [44, 45]:

$$F_s(t) \equiv \langle \exp[i\mathbf{k} \cdot \mathbf{X}(t)] \rangle \quad (6)$$

as a function of time for $|\mathbf{k}| = \pi/(8b)$. The average is performed over all the angles of the wavevector \mathbf{k} and over all the nodes. For a fluid $F_s(t) \rightarrow 0$ exponentially fast at late times; for a solid $F_s(t)$ goes to a non-zero

constant at late times. Again, we find a transition from fluid to a solid at a critical value $\Phi = \Phi_c$.

Next we study the response of the membrane to imposed linear shear strain. We deform the frame such that a point at location x, y on the frame is displaced by $Sy, 0$. The strain of the frame is given by S . In Fig. (4A) we plot the change in energy of the membrane ΔE as a function of time for different values of Φ and for a single strain. The energy is maximum at $t = 0$. As time progresses the energy relaxes and at late times reaches a constant value ΔE_∞ with fluctuations. For $\Phi < \Phi_c$ we find that the membrane relaxes such that at late time $\Delta E_\infty = 0$. In other words, there is no energy cost to shear strain. These are examples of a (two dimensional) fluid membrane. But for $\Phi > \Phi_c$ at late times the ΔE_∞ reaches a constant non-zero value (with thermal fluctuations). This is a feature of solid membranes which can sustain shear strain. In Fig. (4B) we plot the change in energy at late times, ΔE_∞ , as a function of Φ for different values of strain, S . For $\Phi < \Phi_c$, ΔE_∞ is zero for all strains. For $\Phi > \Phi_c$, ΔE_∞ is finite and also increases with S . In Fig. (4C) we plot ΔE_∞ as a function of S^2 for different values of Φ . We obtain $\Delta E_\infty \propto S^2$, the constant of proportionality is the effective shear modulus μ which depends on Φ .

In Fig. (5A), we plot both the diffusivity obtained from Fig. (3A) and the shear modulus μ obtained from Fig. (4C) as a function of the area fraction Φ_c . We measure D in units of $D(\Phi = 0)$ and measure μ in units of $\mu_s \equiv \mu(\Phi = 1)$ – the shear modulus of the solid membrane. As Φ increases D decreases with $D \approx 0$ for $\Phi > \Phi_c$

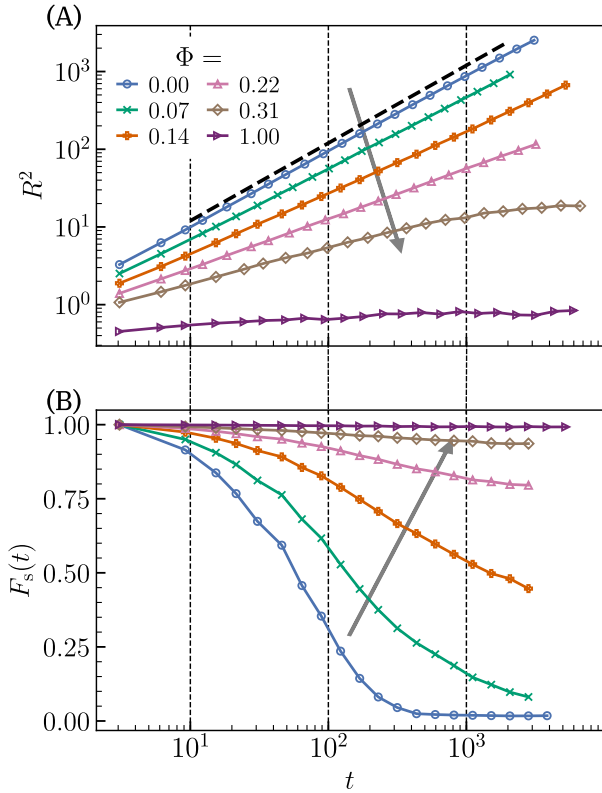


FIG. 3. (A) Log-log plot of the mean-squared-displacement $\langle R^2 \rangle$ as a function of t measured in the units of τ . (B) The function F_s as a function of time t . The arrow points to the direction of the increase in Φ .

with $\Phi_c \approx 0.22$. Simultaneously $\mu \approx 0$ for $\Phi < \Phi_c$. The shear modulus μ increases as Φ increases beyond Φ_c . There is a very tiny range of Φ around Φ_c for which both μ and D are non-zero although both are much smaller than unity. We conclude that there is a transition of the membrane from fluid behavior to solid at $\Phi = \Phi_c$, characterized by the measurement of diffusion constant and the shear modulus. This is a typical rigidity transition. The membrane is either a solid ($\Phi > \Phi_c$) or a fluid ($\Phi < \Phi_c$) – it does not have the dual nature – both a solid and a fluid – exhibited by cell membranes.

We now introduce the second novelty in our model. For all the cases where Φ is not equal to zero or unity, i.e., for the cases where there are both solid and fluid nodes in the model, we introduce a harmonic pinning potential that pins (anchors) only the solid points to the x_1 - x_2 plane. The additional term in the energy of the membrane is

$$E_{\text{pin}} = \sum_{i=s} \frac{K}{2} (\mathbf{X}_i - \mathbf{X}_i^0)^2, \quad (7)$$

where the suffix ‘s’ denotes the solid points. The vector \mathbf{X}_i^0 is the initial position of the i -th node and K the spring constant of the pinning potential. The goal

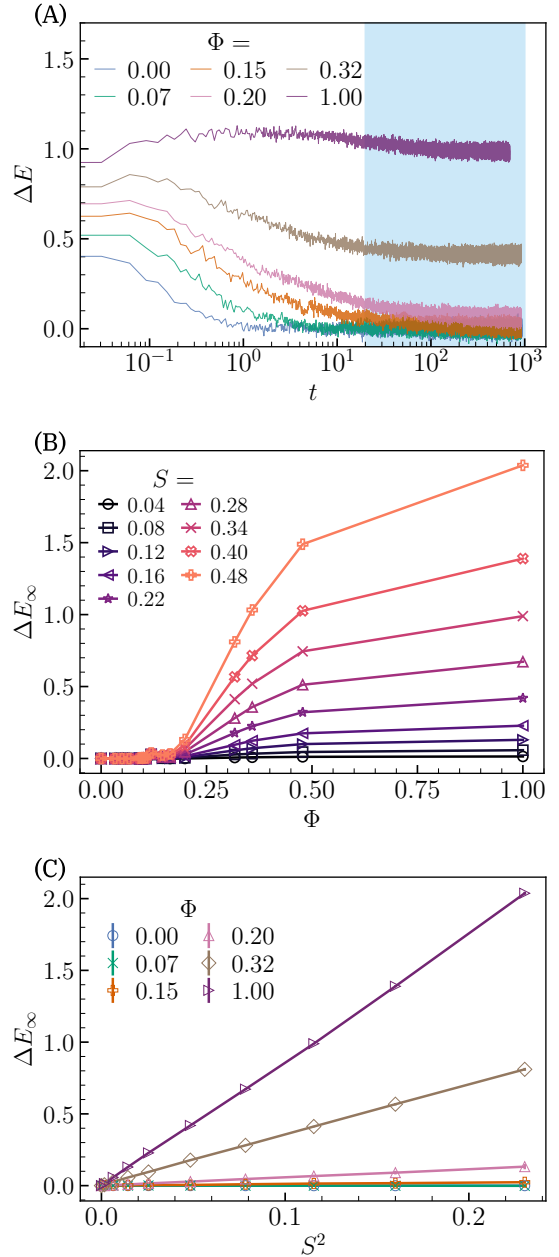


FIG. 4. (A) The change in energy, ΔE , of the sheared membrane as a function of non-dimensional time, for different values of Φ and constant shear strain $S = 0.34$. The area fraction Φ increases from bottom to top. The mean energy at late times is ΔE_∞ , (calculated as an average over the shaded region) which is a function of both S and Φ . (B) The change in energy at late times, ΔE_∞ , as a function of Φ for different values of S . For Φ smaller than certain critical value $\Phi_c \approx 0.23$, $\Delta E_\infty = 0$ for all values of S . (C) The change in energy at late times, ΔE_∞ , as a function of S^2 for different values of Φ . For $\Phi < \Phi_c$, $\Delta E_\infty = 0$. The slopes of these lines are the effective shear modulus $\mu(\Phi)$. The errorbars in (B) and (C) are smaller than the size of the symbols.

is to mimic the attachment of the membrane to the cytoskeleton. In Fig. (5B) we show a typical snapshot of the sheared *pinned* membrane. We find that the pinning has no effect on $\langle R^2 \rangle$, it is indistinguishable from $\langle R^2 \rangle$ of the unpinned membrane (see Appendix B). Consequently the lateral diffusion coefficient depends on Φ alone – it is independent of whether the solid points are pinned or not. But, pinning significantly changes the shear modulus μ . To Fig. (5A) we now add the plot of μ [normalized by $\mu(\Phi = 1)$] for the pinned membrane as a function of Φ . For $\Phi > 0.04$ the the pinned membrane has a non-zero μ . The shear modulus of the pinned membrane is always higher than the unpinned one. Remarkably there is a large range of values of Φ , $0.04 < \Phi < 0.2$ over which the membrane is a fluid, characterized by the diffusivity of its nodes, but also solid if the shear elastic modulus μ is measured. This range of Φ is shaded in Fig. (5A). We have now reached our goal, a minimal model of the cell membrane that can capture both its solid and fluid aspects.

How does pinning affect bending and area modulus of the membrane? The bending modulus is not affected by pinning. To show this, we calculate the power-spectra of height fluctuations:

$$G(q) = \langle f(\mathbf{q})f(-\mathbf{q}) \rangle. \quad (8)$$

At large q we obtain $G(q) \sim \kappa q^4$ where the bending modulus κ is the same for all area fraction Φ , (see Appendix C 1). Note that pinning does change $G(q)$ at small q : for the solid and the fluid membrane, none of which are pinned, $G(q) \sim q^2$ at small q whereas for the pinned membranes $G(q)$ becomes almost independent of q as Φ increases.

The area modulus can be written as a function of the two Lamé coefficients: $K_a = 2(\mu + \lambda)$, of which we have already calculated μ . To calculate λ we deform our frame such that its shape remains the same (a square) but the area changes. The change in energy of the membrane at late times gives λ . As expected, we find that both the (unpinned) solid and fluid membrane shows the same response to stretching; pinning increases K_a (see Appendix C).

In summary, in this paper we introduce a model of membrane that has physical properties akin to both solids and fluids. In particular, within a certain parameter range, the fluid nodes of the membrane show (anomalous) diffusion while the membrane as a whole have a non-zero elastic shear modulus. The key contribution to the elastic shear modulus comes from the pinning of the solid nodes to a flat surface. We emphasize that although motivation behind our model is the cell membrane, we do not attempt to capture all the incredible complexity of natural biological membranes in this model. A simpler experimental analog of our model is a giant unilamellar vesicle (GUV) with cytoskeleton [37, 46–49] – a step towards building synthetic cells. In such composite systems, also in cells, the coupling of the cytoskeleton to the membrane can be tuned. Experiments [47] show that in-

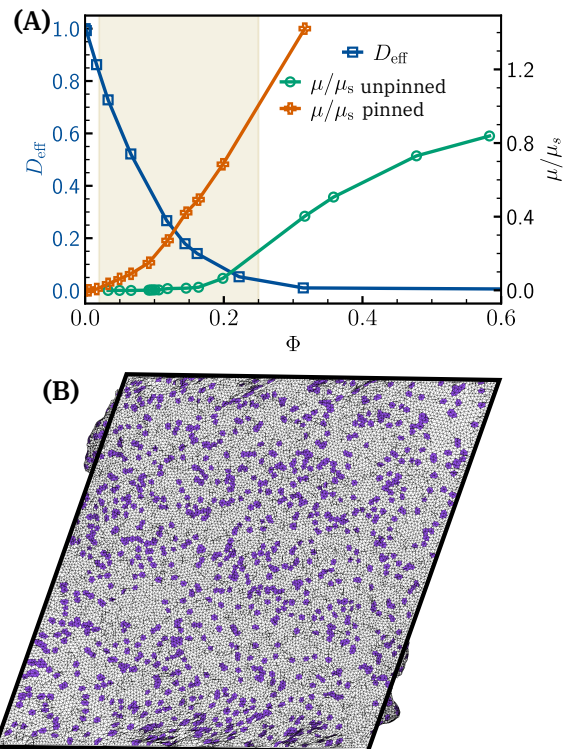


FIG. 5. (A) The diffusion coefficient D , (left axis) and the effective shear modulus μ (right axis) as a function of area fraction Φ . The coefficient D is normalized by the diffusivity of the fluid membrane, $D(0)$. The shear modulus μ is normalized by the shear modulus of the solid membrane μ_s . The diffusion coefficient is zero for $\Phi > \Phi_c$, with $\Phi_c \approx 0.23$. The shear modulus is zero for $\Phi < \Phi_c$. Both of them show a rigidity transition at $\Phi = \Phi_c$. The diffusivity of the pinned membrane (not shown here) is equal (within error bars) to the non-pinned one. The orange curve shows μ/μ_s for the pinned membrane, for which $\mu > 0$ for $\Phi \gtrsim 0.04$. Thus for $0.04 < \Phi < \Phi_c$, the shaded region, the pinned membrane has physical properties akin to both solids and fluids. The error bars in the data are smaller than the size of the symbols. (B) A typical snapshot of the strained pinned membrane for $\Phi = 0.2$ and $S = 0.34$.

clusion of cytoskeleton has minimal effect on the bending modulus (measured by the fluctuation spectrum of height field). We find the same negative result. A different technique (hydrodynamic tube-pulling) shows that the effective cortical tension increases [50]. The tension is proportional to the area modulus K_a which in our model does increase. To the best of our knowledge, the effective shear modulus of such systems have not been measured yet. Note that, while comparing our model with these experiments we expect at best a qualitative agreement because we do not take into account either the active nature of the cytoskeleton or its viscoelastic property. It is straightforward to include activity and study how it influences the mechanical properties in our model along the lines described in Refs. [31].

From the point of view of soft matter physics, our model describes an exotic two dimensional material with physical properties akin to both solids and fluids.

ACKNOWLEDGMENTS

We thank Vipin Agrawal, Bidisha Sinha and Ananyo Maitra for discussions. The figures in this paper are

plotted using the free software matplotlib [51]. We use FFTW [52] for fast Fourier transform. DM acknowledges the support of the Swedish Research Council Grant No. 638-2013-9243 and 2016-05225. The simulations were enabled by resources provided by the Swedish National Infrastructure for Computing at PDC partially funded by the Swedish Research Council through grant agreement no. 2018-05973.

-
- [1] Allison D. Dupuy and Donald M. Engelman, “Protein area occupancy at the center of the red blood cell membrane,” *Proceedings of the National Academy of Sciences* **105**, 2848–2852 (2008).
- [2] S. J. Singer and Garth L. Nicolson, “The fluid mosaic model of the structure of cell membranes,” *Science* **175**, 720–731 (1972).
- [3] Wolfgang Helfrich, “Elastic properties of lipid bilayers: theory and possible experiments,” *Zeitschrift für Naturforschung c* **28**, 693–703 (1973).
- [4] Marcus Müller, Kirill Katsov, and Michael Schick, “Biological and synthetic membranes: What can be learned from a coarse-grained description?” *Physics Reports* **434**, 113–176 (2006).
- [5] Rob Phillips, Jane Kondev, Julie Theriot, Hernan G Garcia, and Nigel Orme, *Physical biology of the cell* (Garland Science, 2012).
- [6] Heinz J Deuling and Wolfgang Helfrich, “Red blood cell shapes as explained on the basis of curvature elasticity,” *Biophysical journal* **16**, 861–868 (1976).
- [7] HJ Deuling and W Helfrich, “The curvature elasticity of fluid membranes: a catalogue of vesicle shapes,” *Journal de Physique* **37**, 1335–1345 (1976).
- [8] C. Pozrikidis, “Resting shape and spontaneous membrane curvature of red blood cells,” *Mathematical Medicine and Biology* **22**, 34–52 (2005).
- [9] Gerald Lim HW, Michael Wortis, and Ranjan Mukhopadhyay, “Stomatocyte–discocyte–echinocyte sequence of the human red blood cell: Evidence for the bilayer–couple hypothesis from membrane mechanics,” *Proceedings of the National Academy of Sciences* **99**, 16766–16769 (2002).
- [10] Jonathan B Freund, “Numerical simulation of flowing blood cells,” *Annual review of fluid mechanics* **46**, 67–95 (2014).
- [11] Sylvie Henon, Guillaume Lenormand, Alain Richert, and Francois Gallet, “A new determination of the shear modulus of the human erythrocyte membrane using optical tweezers,” *Biophysical journal* **76**, 1145–1151 (1999).
- [12] Ming Dao, Chwee Teck Lim, and Subra Suresh, “Mechanics of the human red blood cell deformed by optical tweezers,” *Journal of the Mechanics and Physics of Solids* **51**, 2259–2280 (2003).
- [13] S. Suresh, “Mechanical response of human red blood cells in health and disease: Some structure-property-function relationships,” *Journal of Materials Research* **21**, 1871–1877 (2006).
- [14] G. Bao and S. Suresh, “Cell and molecular mechanics of biological materials,” *Nature Materials* **2**, 715–725 (2003).
- [15] A Ishihara, Y Hou, and K Jacobson, “The thy-1 antigen exhibits rapid lateral diffusion in the plasma membrane of rodent lymphoid cells and fibroblasts.” *Proceedings of the National Academy of Sciences* **84**, 1290–1293 (1987).
- [16] Ken Ritchie, Ryota Iino, Takahiro Fujiwara, Kotono Murase, and Akihiro Kusumi, “The fence and picket structure of the plasma membrane of live cells as revealed by single molecule techniques,” *Molecular membrane biology* **20**, 13–18 (2003).
- [17] Peter S James, Conor Hennessy, Torunn Berge, and Roy Jones, “Compartmentalisation of the sperm plasma membrane: a frap, flip and spfi analysis of putative diffusion barriers on the sperm head,” *Journal of cell science* **117**, 6485–6495 (2004).
- [18] Kotono Murase, Takahiro Fujiwara, Yasuhiro Umemura, Kenichi Suzuki, Ryota Iino, Hidetoshi Yamashita, Mihoko Saito, Hideji Murakoshi, Ken Ritchie, and Akihiro Kusumi, “Ultrafine membrane compartments for molecular diffusion as revealed by single molecule techniques,” *Biophysical Journal* **86**, 4075–4093 (2004).
- [19] Akihiro Kusumi, Chieko Nakada, Ken Ritchie, Kotono Murase, Kenichi Suzuki, Hideji Murakoshi, Rinshi S. Kasai, Junko Kondo, and Takahiro Fujiwara, “Paradigm shift of the plasma membrane concept from the two-dimensional continuum fluid to the partitioned fluid: High-speed single-molecule tracking of membrane molecules,” *Annual Review of Biophysics and Biomolecular Structure* **34**, 351–378 (2005).
- [20] Suliana Manley, Jennifer M Gillette, George H Patterson, Hari Shroff, Harald F Hess, Eric Betzig, and Jennifer Lippincott-Schwartz, “High-density mapping of single-molecule trajectories with photoactivated localization microscopy,” *Nature methods* **5**, 155–157 (2008).
- [21] Aubrey V. Weigel, Blair Simon, Michael M. Tamkun, and Diego Krapf, “Ergodic and nonergodic processes coexist in the plasma membrane as observed by single-molecule tracking,” *Proceedings of the National Academy of Sciences* **108**, 6438–6443 (2011).
- [22] Diego Krapf, “Mechanisms underlying anomalous diffusion in the plasma membrane,” *Current topics in membranes* **75**, 167–207 (2015).
- [23] Zheng Shi, Zachary T Graber, Tobias Baumgart, Howard A Stone, and Adam E Cohen, “Cell membranes resist flow,” *Cell* **175**, 1769–1779 (2018).
- [24] This is different from modeling a cell as a porous media.
- [25] Richard P Feynman, Robert B Leighton, and Matthew Sands, *The Feynman Lectures on Physics: Mainly Electromagnetism and Matter, Vol. 2* (Addison-Wesley,

- Reading, reprinted, 1977).
- [26] LD Landau and EM Lifshitz, *Theory of Elasticity*, Course of Theoretical Physics, Vol. 7 (Pergamon Press Ltd., Oxford, England, 1970).
- [27] G Gompper and DM Kroll, “Triangulated-surface models of fluctuating membranes,” in *Statistical mechanics of membranes and surfaces*, edited by David Nelson, Tsvi Piran, and Steven Weinberg (World Scientific, 2004) pp. 359–426.
- [28] Jayson Paulose, Gerard A Vliegenthart, Gerhard Gommer, and David R Nelson, “Fluctuating shells under pressure,” *Proceedings of the National Academy of Sciences* **109**, 19551–19556 (2012).
- [29] Thorsten Auth, Dmitry A Fedosov, and Gerhard Gommer, “Simulating membranes, vesicles, and cells,” in *The Giant Vesicle Book* (CRC Press, 2019) pp. 169–193.
- [30] Vipin Agrawal, Vikash Pandey, Hanna Kylhammar, Apurba Dev, and Dhruvaditya Mitra, “Memc: A package for monte carlo simulations of spherical shells,” *Journal of Open Source Software* **7**, 4305 (2022).
- [31] Vipin Agrawal, Vikash Pandey, and Dhruvaditya Mitra, “Active buckling of pressurized spherical shells: Monte carlo simulation,” *Physical Review E* **108**, L032601 (2023).
- [32] Hyunjune Sebastian Seung and David R Nelson, “Defects in flexible membranes with crystalline order,” *Physical Review A* **38**, 1005 (1988).
- [33] C Itzykson, in *Proceedings of the GIFT seminar, Jaca 85*, edited by J *et al* Abad (World Scientific Singapore, 1986) pp. 130–188.
- [34] Pankaj Mehta, Marin Bukov, Ching-Hao Wang, Alexandre GR Day, Clint Richardson, Charles K Fisher, and David J Schwab, “A high-bias, low-variance introduction to machine learning for physicists,” *Physics reports* **810**, 1–124 (2019).
- [35] Nicholas L Andrews, Keith A Lidke, Janet R Pfeiffer, Alan R Burns, Bridget S Wilson, Janet M Oliver, and Diane S Lidke, “Actin restricts fcepsilon ri diffusion and facilitates antigen-induced receptor immobilization,” *Nature cell biology* **10**, 955–963 (2008).
- [36] Fabian Heinemann, Sven K Vogel, and Petra Schwille, “Lateral membrane diffusion modulated by a minimal actin cortex,” *Biophysical journal* **104**, 1465–1475 (2013).
- [37] Tobias Härtel and Petra Schwille, “Giant unilamellar vesicles with cytoskeleton,” in *The Giant Vesicle Book* (CRC Press, 2019) pp. 53–70.
- [38] Ralf Metzler and Joseph Klafter, “The random walk’s guide to anomalous diffusion: a fractional dynamics approach,” *Physics reports* **339**, 1–77 (2000).
- [39] S. Condamin, V. Tejedor, R. Voituriez, O. Bénichou, and J. Klafter, “Probing microscopic origins of confined subdiffusion by first-passage observables,” *Proceedings of the National Academy of Sciences* **105**, 5675–5680 (2008).
- [40] Felix Höfling and Thomas Franosch, “Anomalous transport in the crowded world of biological cells,” *Reports on Progress in Physics* **76**, 046602 (2013).
- [41] Teresa Bauer, Felix Höfling, Tobias Munk, Erwin Frey, and Thomas Franosch, “The localization transition of the two-dimensional lorentz model,” *The European Physical Journal Special Topics* **189**, 103–118 (2010).
- [42] M.J. Saxton, “Anomalous diffusion due to obstacles: a monte carlo study,” *Biophysical Journal* **66**, 394–401 (1994).
- [43] Bong June Sung and Arun Yethiraj, “Lateral diffusion and percolation in membranes,” *Phys. Rev. Lett.* **96**, 228103 (2006).
- [44] Léon Van Hove, “Correlations in space and time and born approximation scattering in systems of interacting particles,” *Physical Review* **95**, 249–262 (1954).
- [45] Dapeng Bi, Xingbo Yang, M. Cristina Marchetti, and M. Lisa Manning, “Motility-driven glass and jamming transitions in biological tissues,” *Physical Review X* **6** (2016), 10.1103/physrevx.6.021011.
- [46] Michael Murrell, Léa-Laetitia Pontani, Karine Guevorkian, Damien Cuvelier, Pierre Nassoy, and Cécile Sykes, “Spreading dynamics of biomimetic actin cortices,” *Biophysical journal* **100**, 1400–1409 (2011).
- [47] Feng-Ching Tsai, Björn Stuhmann, and Gijse H Koenderink, “Encapsulation of active cytoskeletal protein networks in cell-sized liposomes,” *Langmuir* **27**, 10061–10071 (2011).
- [48] Sven K Vogel, Fabian Heinemann, Grzegorz Chwastek, and Petra Schwille, “The design of macs (minimal actin cortices),” *Cytoskeleton* **70**, 706–717 (2013).
- [49] Allen P Liu and Daniel A Fletcher, “Biology under construction: in vitro reconstitution of cellular function,” *Nature Reviews Molecular Cell Biology* **10**, 644–650 (2009).
- [50] Karine Guevorkian, John Manzi, Léa-Laetitia Pontani, Françoise Brochard-Wyart, and Cécile Sykes, “Mechanics of biomimetic liposomes encapsulating an actin shell,” *Biophysical journal* **109**, 2471–2479 (2015).
- [51] J. D. Hunter, “Matplotlib: A 2d graphics environment,” *Computing in Science & Engineering* **9**, 90–95 (2007).
- [52] Matteo Frigo and Steven G. Johnson, “The design and implementation of FFTW3,” *Proceedings of the IEEE* **93**, 216–231 (2005), special issue on “Program Generation, Optimization, and Platform Adaptation”.

Appendix A: Details of simulation

N	65536 (diffusion expt.) 16384 (shear expt.)
H	10^4
κ	4.0
Φ	0.0, 0.002, 0.017, 0.034, 0.051, 0.068, 0.094, 0.12, 0.14, 0.17, 0.21, 0.31, 0.35, 0.48
S	0.04, 0.08, 0.12, 0.16, 0.22, 0.28, 0.34, 0.40, 0.48
K	200

TABLE I. The parameters used in our simulations: N is the total number of nodes; H is spring constant of the harmonic spring that connects to neighbouring nodes; κ is the bending modulus; Φ is the area fraction occupied by the solid nodes; S is the externally imposed strain on the frame; K is the spring constant of the harmonic pinning potential. Our production runs are typically for 10^6 Monte Carlo steps. The length of a side of the square frame is $\sqrt{N}b$ where b , the average bond length, is our unit of length. The parameters, H , κ and K are measured in the unit of $k_B T$; N , Φ and S are dimensionless.

Appendix B: Diffusion

The anomalous diffusion observed in a heterogeneous medium like plasma membrane is often attributed to crowding due to macromolecules [22, 40]. The effect of crowding is modeled by confining a random-walker in a space filled with immobile obstacles. This model has been studied in a lattice [42], where certain sites are inaccessible to a walker or in a continuous medium, where a Brownian walker diffuses through the gaps between the obstacles—also known as Lorentz model [41, 43]. As the concentration of the obstacles is increased the walker goes from diffusion to subdiffusion for intermediate times. At very late times the subdiffusive trajectories either become diffusive or gets localized ($D_{\text{eff}} \rightarrow 0$) [41, 42].

There are qualitative similarities between these models and ours. In particular, the fluid nodes corresponds to the Brownian walker while the solid patches act as obstacles. We run two kinds of simulations:

- (A) The solid nodes and the patches around them move around.
- (B) The solid nodes are pinned.

We call the former unpinned (or unanchored) and the latter pinned. It turns out that the diffusive behavior of the fluid nodes is independent of whether the solid nodes are pinned or not. In Fig. (6A) we show the mean-square-displacement ($\langle R^2 \rangle$) of the fluid nodes for the case where the solid nodes are pinned (open symbols) and unpinned (continuous lines). They fall on top of each other.

We interpret this data in two ways. First we consider the transition from diffusion to subdiffusion as Φ , the

area fraction occupied by the solid patches, is changed. We fit the means square displacement (as a function of time) with

$$\langle R^2 \rangle \sim t^\beta \quad (\text{B1})$$

to extract β , where $\beta = 1$ corresponds to diffusion. For $\Phi = 0$ we obtain $\beta = 1$. Beyond a critical value of Φ , Φ_c the trajectories are localized, i.e., $\langle R^2 \rangle$ goes to a constant at late times. It is difficult to determine Φ_c accurately as the diffusion is limited to a fixed box. From our data we estimate $\Phi_c \approx 0.23$. In Fig. (6B) we plot β as a function of Φ/Φ_c . In the same figure, we also compare our results with two earlier works. As the models used in these works cannot be mapped to ours or to each other we identify our Φ with the fraction of inaccessible sites in Ref. [42] and the area occupied by immobile obstacles in Ref. [43]. Our results are not too different from these earlier works. For example, in Ref. [42], Φ_c is the equal to percolation transition of the lattice. Sung and Yethiraj [43] reports $\Phi_c = 0.22$.

The second way to interpret the data of $\langle R^2 \rangle$ as a function of time is to calculate a Φ dependent diffusivity

$$D(\Phi) \equiv \lim_{t \rightarrow \infty} \frac{\langle R^2 \rangle}{t}, \quad (\text{B2a})$$

$$\text{and } D_{\text{eff}} \equiv \frac{D(\Phi)}{D(\Phi = 0)}, \quad (\text{B2b})$$

the effective diffusivity. We plot D_{eff} as a function of Φ in Fig. (6C). For the Lorentz model,

$$D_{\text{eff}} \sim \left(\frac{\Phi_c - \Phi}{\Phi_c} \right)^\gamma \quad (\text{B3})$$

with $\gamma \approx 1.33$ [41]. It is not clear from our data whether we see such a behavior. We plot D_{eff} as a function of Φ in both a log–lin plot Fig. (6C) and a log–log plot Fig. (6D). The precise dependence of D_{eff} near $\Phi \approx \Phi_c$ is not central to our work. We leave it for a future investigation.

1. Waiting time distribution

The underlying mechanism for the anomalous diffusion can be described by various theoretical models such as fractional Brownian motion (fBM), and continuous time random walk (CTRW) [38–40]. In CTRW, the time taken by a walker to take a step is not constant but is drawn from a distribution which has a power-law tail. The exponent characterizing this waiting time distribution determines to the exponent of the mean square displacement, β [38].

The exponent of the waiting time distribution can be estimated by studying the first passage time statistics [39]. From the trajectory of fluid nodes we calculate the cumulative probability distribution function, \mathcal{Q} , of the first passage time T_{fp} , which defined as time taken

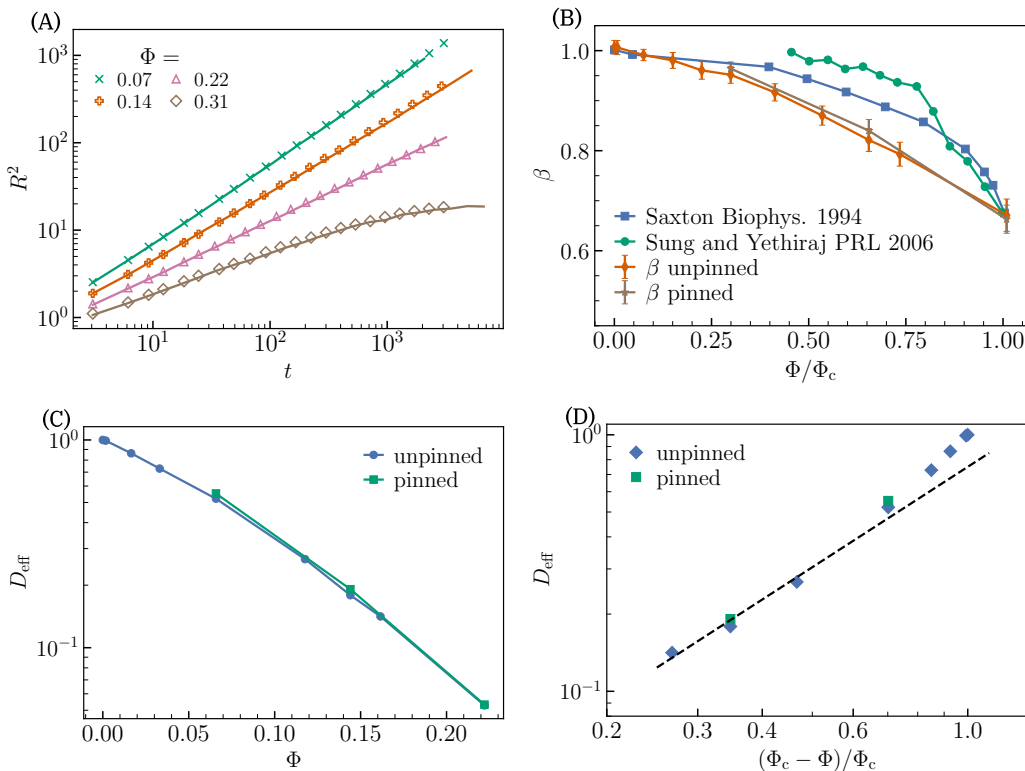


FIG. 6. (A) Comparison of mean square displacement, of the fluid point, between the two cases: (A) solid nodes are pinned (symbols) and (B) they are unpinned (lines). (B) The exponent β as obtained from mean square displacement. For comparison we overlay the data obtained by Sung and Yethiraj [43] and Saxton [42]. (C) Semi-log plot of D_{eff} versus Φ . (D) Log-log plot of D_{eff} versus $(\Phi_c - \Phi)/\Phi_c$. The dashed line, with an exponent 1.33 is the corresponding scaling relation for the Lorentz model.

by a fluid particle to exit a circle of radius $11b$ for the first time. We plot the distribution in Fig. (7A) in log-log scale. It is clear that the tails are not power laws. The same behavior was also observed in the model of Ref [43]. The tail of the Q can be best approximated by an exponential, see Fig. (7B) which implies the probability distribution of T_{fp} also have an exponential tail.

Appendix C: Measurement of elastic constants

We measure the two Lamé coefficients λ and μ by deforming all the in-plane coordinates, including the coordinates for the frame. This increases the total energy for the membrane. We then hold the frame fixed and let the membrane evolve through Monte Carlo steps.

To measure μ we do the following deformation:

$$\begin{bmatrix} x_1 \\ x_2 \end{bmatrix} \rightarrow \begin{bmatrix} x_1 \\ x_2 \end{bmatrix} + \begin{bmatrix} 0 & S \\ 0 & 0 \end{bmatrix} \begin{bmatrix} x_1 \\ x_2 \end{bmatrix}, \quad (\text{C1})$$

To measure λ we perform the following deformation.

$$\begin{bmatrix} x_1 \\ x_2 \end{bmatrix} \rightarrow \begin{bmatrix} x_1 \\ x_2 \end{bmatrix} + \begin{bmatrix} \Sigma & 0 \\ 0 & \Sigma \end{bmatrix} \begin{bmatrix} x_1 \\ x_2 \end{bmatrix}. \quad (\text{C2})$$

to achieve uni-axial expansion. The two deformation are shown in Fig. (8A).

We show the change in energy relative to the initial configuration at late times, ΔE_∞ versus Σ in Fig. (8B). We find that both solid and fluid membrane show the same response to stretching. We note that the ΔE_∞ is larger, at same Σ , for the cases of pinned membrane which implies K_a increases with pinning.

1. Measurement of bending modulus

We remind the reader the theory of elasticity of an isotropic and homogeneous two-dimensional elastic material. In the Monge gauge the deformations can be described by an in-plane vector $\mathbf{u}(x_1, x_2)$ and an out-of-plane displacement $f(x_1, x_2)$. The Hamiltonian is given by

$$\mathcal{H} = \int d\mathbf{x} \left[\frac{\kappa}{2} (\nabla^2 f)^2 + \mu s_{\alpha\beta}^2 + \frac{\lambda}{2} s_{\alpha\alpha}^2 \right], \quad (\text{C3a})$$

$$\text{where } s_{\alpha\beta} \equiv \frac{1}{2} (\partial_\alpha u_\beta + \partial_\beta u_\alpha + \partial_\alpha f \partial_\beta f), \quad (\text{C3b})$$

is the strain tensor and μ and λ are the two Lamé coefficients [25, 26].

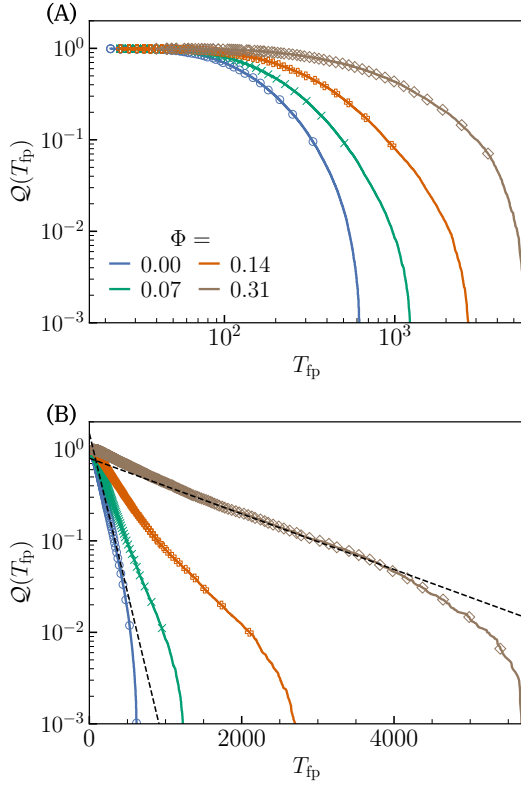


FIG. 7. (A) Log-log and (B) semi-log plot of the cumulative distribution function $\mathcal{Q}(T_{fp})$ of the first-passage-time T_{fp} , for different Φ . The dashed lines in panel (B) indicates $\exp(-CT_{fp})$, where C is chosen to best fit the curves.

We calculate the spectra for the out of plane fluctuations $f(\mathbf{x})$ where the in-plane co-ordinates $\mathbf{x} = (x_1, x_2)$. For small fluctuations, the power spectra for the fluctuations, $G(q)$, is given by,

$$G(q) = \frac{Ak_B T}{(\kappa q^4 + \sigma q^2)}, \quad (\text{C4})$$

where A is the area of the projection of the membrane on to the x_1 - x_2 plane., κ is the bending modulus and $\sigma = (\mu + \lambda) \langle [\mathcal{A}_i / \mathcal{A}_i(t=0) - 1] \rangle$ is the effective tension [5]. We show the fluctuation spectra from our simulations in Fig. (9). For both $\Phi = 0$ (fluid membrane) and $\Phi = 1$ (solid membrane) we can identify both the κq^4 at large q and σq^2 at small q . At intermediate Φ , the q^2 scaling disappears as solid regions are pinned to the substrate.

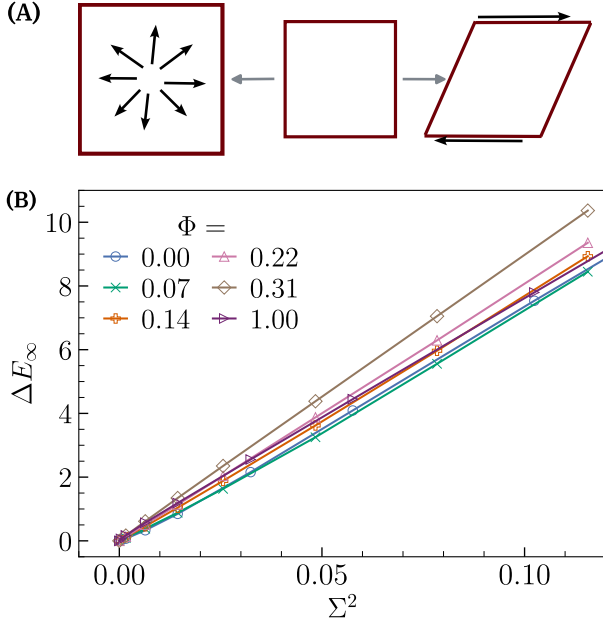


FIG. 8. (A) The deformation of the frame: Middle figure shows the undeformed frame, left shows uni-axial stretching and right shows shear deformation. The frame is held fixed and the points in the membrane are allowed to relax via Monte Carlo steps. (B) The change in energy relative to the initial configuration at late times, ΔE_∞ as a function of the Σ^2 .

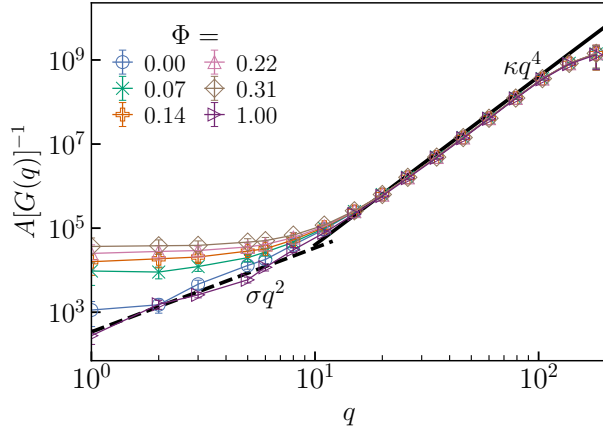


FIG. 9. Log-log plot of the power spectra of the height fluctuations. The black dashed line shows the σq^2 and the κq^4 scaling is shown using a continuous line of the same color.